

A Novel Fuzzy C-Means Clustering Framework for Accurate Road Crack Detection: Incorporating Pixel Augmentation and Intensity Difference Features

Munish Bhardwaj¹, Nafis Uddin khan², Vikas Baghel¹

¹Jaypee University of Information Technology, Solan, India

²SR University Warangal, India

munish368@gmail.com, nafis.khan@sru.edu.in, vikas.baghel@juit.ac.in

Keywords: K-means clustering, fuzzy C-means clustering, road crack detection

Received: September 5, 2024

The widespread occurrence of fractures in roads globally threaten traffic safety and demand substantial annual maintenance costs. Expenses can be substantially reduced by detecting fractures promptly, however manual methods are less rapid and inaccurate. Although automatic crack detection offers efficiency, but challenges like low contrast and background noise in pictures can impact its accuracy. To address these obstacles, this study proposes a potent Fuzzy C-Means clustering technique to enhance automated fracture detection. This approach employs pixel augmentation through a scaling factor to improve pixel details by examining the ratios from individual to cumulative values. Additionally, it considers the sum of the total ratio value and the minimum-to-maximum intensity within a 3x3 window, prior to segmentation. Moreover, the method identifies intrinsic pixel connections through absolute intensity differences, supporting crack detection. It also effectively detects cracks from unfamiliar images across diverse scenarios, without the need for a training dataset. According to experimental results, an enhanced Fuzzy C-Means Clustering approach for road crack detection, achieving superior precision, recall, and F1 scores (86.68, 88.53, 87.59) compared to K-Means Clustering (76.82,78.05,77.43), Fuzzy C-Means Clustering (79.76,80.72,80.23), and Manhattan distance based fuzzy C-Means clustering (84.09, 86.14,85.10). Additionally, it also reduces iteration counts, ensuring computational efficiency. These results validate its robustness and effectiveness, making it a promising solution for automated road crack detection systems.

Povzetek: Predlagan je nov okvir gručenja Fuzzy C-Means (FCM) za natančno zaznavanje razpok na cestah, ki vključuje povečanje slikovnih pik in značilnosti razlike v intenzivnosti. Ta pristop izboljšuje podrobnosti slikovnih pik z uporabo faktorja skaliranja in upošteva razliko v intenzivnosti med slikovnimi pikami. Predlagana metoda učinkovito zazna razpoke na različnih cestnih slikah brez potrebe po učnem naboru podatkov in dosega boljšo natančnost v primerjavi s tradicionalnimi metodami gručenja.

1 Introduction

Cracks impair the operation of roads and are often caused by decades of age, terrain or topographical conditions, and excessive traffic. Hence, it becomes imperative to acquiring precise statistics on road fractures [1], which can be accomplished using either hand-executed or automated process. The process of manually recognising fractures is tedious and prone to errors. It is therefore essential to proliferate automatic fracture recognising protocols. These automated methods provide crack information more quickly and precisely [2][3][4]. In addition, these automated methods may also be utilised to find fractures in a range of infrastructure such as hills, underground passageways, reservoirs, and Viaducts [1]. Therefore, to develop an algorithm for automatic road crack detection from images, a comprehensive understanding of how to identify road fractures in photographs is vital.

The crack detecting technique is representing in Figure 1 (road image taken from self-collected

dataset). To initiate this approach, take photographs of the road portions where fractures are expected to be discovered with a camera or similar instrument [2]. Pre-processing should then be applied to the captured photos. The goal of pre-processing is to get rid of any unwanted components from the photographs that can degrade their quality. These artifacts can be eliminated, allowing for speedy and effective further processing of the image. The image must be converted to grayscale as one of the basic pre-processing stages. After this conversion is finished, a variety of filtering methods can be used to successfully remove unnecessary pixels. After the pre-processing phase, segmentation is applied to the images. In order to extract the precise features of interest from the raw photos, image segmentation is a vital step. There are many picture segmentation methods that are effective in separating regions with the same pixel characteristics [5]. Thus, clustering is found to be the best technique for separating comparable pixels from raw images that indicate the existence of specific traits of interest [5][6].

Therefore, the utilization of clustering techniques, such as K-means clustering (KMC) approach [7][8], the fuzzy C-means clustering (FCMC) method [9][4], Manhattan distance based fuzzy C-Means clustering (MHFCM) algorithm [10] will enable the extraction of road crack patterns from images, as further elucidated in Section II.

Therefore, based on the insights gained from these studies, the primary objective of the proposed approach is to develop an innovative and robust FCM clustering (PIEFCMC) approach that can autonomously identify fractures.

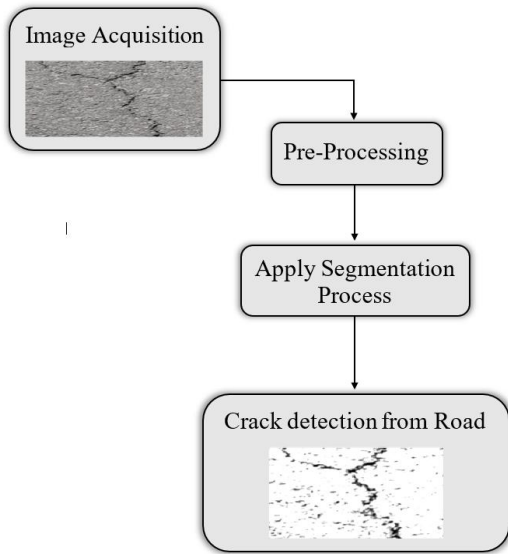


Figure 1. Architecture for road cracks identification utilizing the Image processing Techniques

This is accomplished through the pixel augmentation in 3×3 window and absolute intensity difference between maximum and minimum pixel values which enabling the detection of cracks even in images with low contrast. The suggested approach has been evaluated on a diverse range of road crack photos supplied from a self-compiled dataset. This method's key contributions are as follows:

- 1) The 2-D road pictures data have been processed into 3×3 window ($\tilde{W}_{d(3 \times 3)}$) and it spans on the entire picture.
- 2) The pixel augmentation (P_{aug}) technique has been applying on each window. It utilizes each individual pixel by considering the sum of all values of its neighboring pixels with in $\tilde{W}_{d(3 \times 3)}$.
- 3) In instances where the original pixel values are minimal or approaching zero, the utilization of the total ratio value ($\vartheta_{\tilde{W}_{d(3 \times 3)}}$) serves to accentuate them against the backdrop of background noise.
- 4) Furthermore, the incorporation of the absolute difference enables this methodology viable the exploration of the inherent correlation between the pixels within the road images.

- 5) The outcomes of the experiments exhibit that the suggested robust FCM segmentation approach surpasses KMC, FCMC, and MHFCM in recognizing alligator, transverse, longitudinal fractures, and potholes in real-world road imagery.

The subsequent sections of this paper follow this organization: Section 2 presents a discussion of K-Means, FCM algorithms, and their respective variations. Section 3 elaborates on the proposed algorithm, offering detailed insights. Section 4 showcases the experimental results and discussions, and Section 5 serves as the concluding part of our study and future scope.

2 Related work

A brief overview of conventional and sophisticated FCMC, as well as associated current techniques for road crack identification, are provided in this section

2.1 Fuzzy-C-Means clustering (FCMC)

The FCMC algorithm, devised by Bezdek et al., [9][4] stands as a prominent approach in photo segmentation, leveraging an iterative unsupervised learning approach reminiscent of K-means clustering [12]. In settings devoid of noise, FCM outperforms by endowing every data point with a membership degree across clusters, ultimately determining final cluster values through a combination of centroid proximity and membership strength, ensuring a normalized distribution of memberships [12]. Hence the fundamental functions of the conventional FCMC algorithm can be encapsulated as below [12][23][24]:

1. The objective function of FCM as follows [10]:

$$\mathcal{T}_f(\phi, G) = \sum_{g=1}^t \sum_{l=1}^p \phi_{lg}^b \|X_l - G_g\|^2 \quad (1)$$

Where X_l is finite dataset, p, t is total pixels, clusters, b is fuzzification parameter and G is cluster centers.

2. At the outset the membership matrix (ϕ_{lg}) undergoes random initialization via: $\sum_{g=1}^t \phi_{lg} (= 1)$; where $\phi = [\phi_{lg}]_{t \times p}$ with $0 \leq \phi \leq 1$.

3. Utilize the following equation ascertain G_g

$$G_g = \frac{\sum_{l=1}^p \phi_{lg}^b X_l}{\sum_{l=1}^p \phi_{lg}^b}; \quad g=1, 2, 3, \dots, t \text{ and } b > 1 \quad (2)$$

4. Enhance the ϕ_{lg} & compute the updated ϕ_{lg} using:

$$\phi_{lg} = \frac{\left[\frac{1}{E_{lg}} \right]^{\frac{1}{b-1}}}{\sum_{c=1}^t \left[\frac{1}{E_{lc}} \right]^{\frac{1}{b-1}}} \quad (3)$$

Where E_{lg} is Euclidean distance ($E_{lg} = \|X_l - G_g\|$)

5. The iterative procedure terminates once the $\|\phi^{(j+1)} - \phi^{(j)}\|$ become smaller than the positive threshold, denoted as Ω . Here, j is iteration index.

FCMC algorithms perform admirably in segmenting noise-free photographs but grapple with challenges when confronted with pictures noise and artifacts [12]. This is primarily due to their oversight of nearby pixel relationships, leading to difficulties in managing enumeration time costs [12].

2.2 Utilize in road crack reorganization

The manual road crack detection proves tedious and error-prone, emphasizing the necessity for an algorithm capable of precisely identifying fractures in unseen images amidst varying environmental conditions. FCMC's rise in popularity as an unsupervised clustering technique is evident in its widespread use across diverse image segmentation tasks, demonstrating superior fracture detection in newly captured photos across various environments. Nonetheless, the scarcity of FCMC-based algorithms for automated road fracture detection through photograph segmentation persists. A technique for recognizing cracks in concrete images has been demonstrated by Noh et al. [11]. It involved the utilization of FCMC and multiple noise scarcity strategies for segmentation. However, when considerable noise is present in cluster containing fractures, the accomplishment rate of fracture diagnosis drop significantly. Bhardwaj et al. [12] proposes an advanced FCMC algorithm that automatically detects fractures by incorporating optimal edge pixels using second-order differences and intensity-based fuzzy factors. By utilizing edge and non-edge pixel intensities, the method reliably identifies edges in low-contrast images without the need for training datasets or complex parameter tuning. It effectively detects fractures and surpasses existing methods.

Oumaa et al. [13] apply a multi-scale wavelet transform filtering method to reduce background noise and enhance image smoothness. Subsequently, they implement an improved process for identifying and segmenting potholes, utilizing unsupervised FCMC and morphological refinement techniques. Additionally, their methodology showcases precision in predicting the dimensions and forms of potholes.

Bhar. et al. [10] utilize the MHFCM approach, as elucidated in reference [10], integrating Manhattan distance (d_{Mht}) and histogram equalization (h_{eqn}) within the FCMC framework. The incorporation of d_{Mht} facilitates enhanced precision by evaluating dissimilarity between the dataset and cluster centroids, particularly enhancing cluster differentiation. Moreover, the inclusion of h_{eqn} contributes to enhancing overall photograph contrast. Consequently, this refined FCMC methodology demonstrates efficacy in detecting various types of road fractures in images. The representation of d_{Mht} and h_{eqn} is denoted as:

$$(d_{Mht})_{lg} = |x_l - G_g| \quad (4)$$

Whereas $g = 1, 2, 3, \dots$, t and $l = 1, 2, 3, \dots, p$

$$h_{eqn}(S) = P(x_S) = \frac{T_S}{p} ; 0 \leq S \leq m-1 \quad (5)$$

Whereas m and p are the total number of gray levels and total number of pixels. The T_S is the total number of pixels with the same intensity level S .

While the MHFCM demonstrates adeptness in detecting fractures, it is encumbered by several limitations. Notably, the h_{eqn} procedure operates on the entire image, augmenting overall contrast but potentially sacrificing local information near edges and boundaries. Additionally, both FCM and h_{eqn} require parameter fine-tuning for optimal outcomes, thereby introducing processing challenges within the MHFCM framework. The amalgamation of these processes could exacerbate complexity and prolong processing times, particularly when dealing with large-scale images.

2.3 Other techniques

KMC necessitates a predetermined number of clusters, a task that can be challenging when dealing with intricate or high-dimensional data, as outlined by Bhard et al. [8]. The author Sadia et al. [14] present the road surface cracks are an early sign of pavement deterioration, leading to costly repairs. An automated method using color histogram analysis, K-means clustering, and Otsu thresholding segment 2D road images to detect cracks. The approach effectively reduces noise, preserves edges, and ensures accurate crack detection. Amita at al. [15] the study enhances image quality under overexposed and underexposed conditions by optimizing pixel intensity, entropy, noise, and edge details using a fuzzy approach. Images are mapped to fuzzy sets, and pixel intensity plays a key role in determining membership during fuzzification. The method preserves details, manages uncertainties, and controls sharpness to balance enhancement and noise reduction, ensuring improved visual quality. Cubero et al. [16] introduce novel approaches for swiftly extracting road fractures and illustrate the utilization of this technique to extract essential attributes required for highlighting the fractures. Ultimately, an image is classified employing a decision tree heuristic method.

By comprehending the basic structural characteristics of cracks, Shi et al.'s automated method [17] effectively reduces noise when identifying road fractures. The author Abdulrahman et al. [18] represent the system employs advanced image pre-processing, precise feature extraction, and a robust fuzzy inference mechanism to detect and classify cracks with exceptional accuracy and reliability across key performance metrics. For fracture detection, Wang et al. [19] state that pavement image quality is critical. But these photos frequently have shadows or noises that mimic shadows, which can be from telegraph poles,

Table 1: Summarized the relevant studies related to road crack detection

Sr. No.	Author	Technique	Methodology	Dataset Used	Performance matrix	Key Findings
1.	Wang et al. [4]	Clustering Algorithms	This study evaluates clustering algorithms for pavement crack segmentation, finding mean-shift excels in de-noising under Gaussian noise based on NMI values.	From Internet Sources	RI-Mean :0.6030, NMI- Mean: 0.1529	Algorithms evaluated are sensitive to noise, leading to over-segmentation and misclassification.
2.	Bhard. et al. [10][5]	MHFCMC	The approach incorporates the integration of Manhattan distance and histogram equalization into FCMC.	From online sources	PSNR: 14.26, Execution Time:2.3	Lose local data close to borders and computational complexity
3.	Noh et al. [11]	Fuzzy C-means Clustering	This method employs segmentation, filtering, and morphological operations to remove noise and clutter using masks.	Self-Collected data set	Precision:0.9, Recall:0.8	Accurate identification is hampered by noise-rich fracture clusters.
4.	Oumaa et al. [13]	Fuzzy C-Means Clustering and morphological reconstruction	It integrates multiscale texture-based wavelet filtering with superpixel clustering using FCMC and morphological reconstruction for pothole detection	Self-collected data set	Dice coefficient: 87.5%, Jaccard Index: 77.7%, Sensitivity: 97.6%	It depends on lighting conditions and visual obstructions, which may affect detection accuracy.
5.	Shi et al. [17][5]	Crack Forest	This method combines integral channel features, random structured forests, and a novel crack descriptor for improved detection and noise differentiation.	CFD dataset	Precision:0.8228, Recall: 0.8944, F1 Score: 0.8571	Incapable of precisely extracting complex background fractures.
6.	Chen et al. [21][5]	MANet	MANet uses MobileNet, depth wise convolutions, and hybrid attention to enhance feature importance.	Crack500 and CFD	Precision:0.7634, Recall:0.890, F1 Score: 0.8221	Longer computing times correspond to more complexity.

edifice, foliage, lights/ lamps, and other objects. An image processing technique is presented to overcome this difficulty and extract pavement fractures from shaded picture. Jie et al. [20] enhance the Canny algorithm with a bilateral filter, Sobel operator, and adaptive thresholds. Detection maps are refined morphologically and fused with DeepLabV3+ features to produce the final map. The Table 1 summarized the relevant studies discussed related to road cracks detection.

In order to overcome the limitations of existing methods, a methodology is required that employs a 3×3 window, along with scaling factor for pixel augmentation. This enhances pixel details and visibility prior to segmentation. Additionally, the local neighborhood relationship is used into the segmentation enhances feature extraction, reduces noise, improves clustering and boundary precision. These advanced aforementioned features are incorporated into the proposed algorithm, as detailed in Section 3.

3 Proposed method

In this section, we present a novel and useful method for spotting road fractures. In order to detect the road cracks, we have presented the innovative cracks identification method using Fuzzy C-Means Clustering i.e., PIEFCMC approach. The purpose of this approach is to address the limitations and issues with the existing methods covered in Section II. The Proposed method uses pixel augmentation (\mathbb{P}_{aug}) and absolute intensity difference ($\mathbb{A}_{d(max.,s)}(s)$). The \mathbb{P}_{aug} is crucial for preparing image data for analysis as it enhances finer details, making features more discernible. Therefore, in this approach a 3×3 window ($\mathbb{W}_{d(3 \times 3)}$) is utilized that spans the whole picture (represent in figure 2) along with scaling factor for pixel augmentation (\mathbb{P}_{aug}) which effectively emphasize pixels details. Additionally, the $\mathbb{A}_{d(max.,s)}(s)$ make this approach possible to observe the intrinsic connection between the picture pixels. As a result, it improves contrast between various region or objects in the picture, thereby enhancing clustering and boundary delineation, leading to improved outcomes. Hence, this process has been subtly represented in algorithm 1 & 2. The detail of the \mathbb{P}_{aug} of image using $\mathbb{W}_{d(3 \times 3)}$ for PIEFCMC approach is discussed below:

3.1 3 × 3 Window

The 3×3 window plays a key role in examines the pixels within its frame and utilize them for pixel enhancement. As it slides across the image, it consistently utilized in the enhancement of each pixel, helping to highlight important features, and make cracks more pronounced. This process results in a clearer and more refined image, which is beneficial for tasks such as crack detection and segmentation. Therefore, it is imperative to ensure accuracy when creating this

window. The relevant mathematical expression for the 3×3 window is as follows [22]:

$$\begin{aligned} \tilde{\mathbb{W}}_{d(3 \times 3)} &= [\dot{X}_{\tilde{\alpha}+i, \acute{\alpha}+i}] \quad (6) \\ \text{for } i &= g \text{ to } g + 2 \ \& \ \acute{i} = d \text{ to } d + 2 \\ \text{for } g &= 0, 1, 2, 3, \dots, l - 2 \ \& \\ d &= 0, 1, 2, 3, \dots, t - 2 \end{aligned}$$

where as $\dot{X}_{\tilde{\alpha}+i, \acute{\alpha}+i}$ represents the individual pixels in 3×3 window ($I_{Pixel}(\tilde{\mathbb{W}}_{d(3 \times 3)})$), \tilde{i} & \acute{i} denote the row & column of the $\tilde{\mathbb{W}}_{d(3 \times 3)}$, $\tilde{\alpha}$ & $\acute{\alpha}$ establish the beginning indices or offsets (i.e., $\tilde{\alpha}$ & $\acute{\alpha} = 1$) and l & t is total number of rows & columns of the image. In particular, \acute{i} stands for the columns to the right of $\acute{\alpha}$ and \tilde{i} for the rows down from $\tilde{\alpha}$. Together, $\tilde{\alpha}$ and $\acute{\alpha}$, \tilde{i} and \acute{i} identify an element's precise placement within the window.

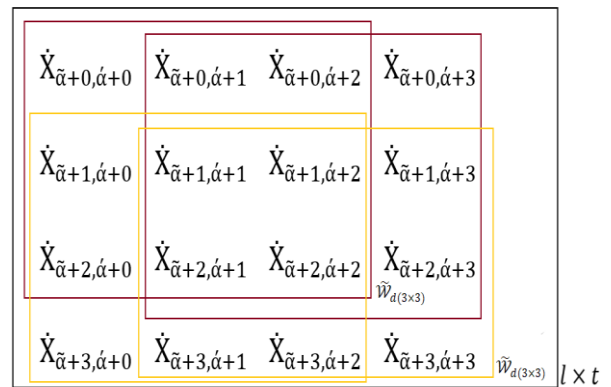


Figure 2: Representation of the 3 × 3 windows and its coverage of surrounding pixels

In Figure 2, the 3×3 window slides across the entire image $l \times t$ (l and t ranging from 0 to 3 for Figure 2), mentioned in table 2. It is also important to understand that the smaller windows (like 2×2), lack sufficient contextual information, making clustering sensitive to noise and ineffective at detecting continuous edges. Conversely, larger windows (4×4 or 5×5 etc.), tend to over-smooth the image, obscuring essential boundaries and fine details. Therefore, a 3×3 window strikes the right balance by reducing noise while preserving critical details, ensuring accurate segmentation and computational efficiency.

3.2 Pixel augmentation of the image using 3 × 3 Window

The Pixel augmentation approach is utilized to enhance the individual pixel values once the $\tilde{\mathbb{W}}_{d(3 \times 3)}$ has been generated. The Figure 2 and Table 2 ensures that all pixels are covered by this window for pixel augmentation. However, the size of $l \times t$ may vary depending on the dimensions of the image being considered.

Table 2: Movement and coverage of the window based on g and d values

Step	Values of g and d for row (i) and column (j)	Position of row (i) and column (j)	Window Coverage
Initial Position	If $g = 0$ and $d = 0$	$i = 0$ to 2 & $j = 0$ to 2	The Window covers the first 9 pixels
Horizontal Movement	If $g = 0$ and $d = 1$	$i = 0$ to 2 & $j = 1$ to 3	The window shifts to the next column
Vertical Movement	If $g = 1$ and $d = 0$	$i = 1$ to 3 & $j = 0$ to 2	The window moves to the next row
Complete Coverage	If $g = 1$ and $d = 1$	$i = 1$ to 3 & $j = 1$ to 3	Window move to the next column and covering all pixels

However, necessary attention is required when determining the augmented scaling factor. Therefore, if the augmented scaling factor ($\tilde{A}\hat{S}_{fa}$) is set excessively large, the picture may exhibit irregular or distorted appearances. While if setting excessively small can lose their precision and sharpness, resulting in a faded or obscured appearance. Therefore, adopting an optimal strategy is essential to maintaining edge quality and improves finer details, making features more visible. Thus, the mathematical expression for augmented image pixels (\mathcal{X}_s) are obtained by considering the values of augmented scaling factor ($\tilde{A}\hat{S}_{fa}$) and individual image pixels [$\check{X}_{\tilde{\alpha}+\tilde{i},\tilde{\alpha}+\tilde{j}}$], may be articulated in the following manner:

$$\mathcal{X}_s = [\tilde{A}\hat{S}_{fa}] \times [\check{X}_{\tilde{\alpha}+\tilde{i},\tilde{\alpha}+\tilde{j}}] \quad (7)$$

The $\tilde{A}\hat{S}_{fa}$ for $\tilde{\mathcal{W}}_{d(3 \times 3)}$ is achieved by utilizing the following mathematical expression:

$$\tilde{A}\hat{S}_{fa} = \check{X}_{\tilde{\alpha}+\tilde{i},\tilde{\alpha}+\tilde{j}} = [\check{R}_{\tilde{\mathcal{W}}_{d(3 \times 3)}} + \vartheta_{\tilde{\mathcal{W}}_{d(3 \times 3)}}] \quad (8)$$

Whereas $\check{R}_{\tilde{\mathcal{W}}_{d(3 \times 3)}} = \left(\frac{I_{Pixel(\tilde{\mathcal{W}}_{d(3 \times 3)})}}{Sum(\tilde{\mathcal{W}}_{d(3 \times 3)})} \right)$ is the ratio of individual pixel ($I_{Pixel(\tilde{\mathcal{W}}_{d(3 \times 3)})}$) value to the sum of all pixels with in 3×3 window ($Sum(\tilde{\mathcal{W}}_{d(3 \times 3)})$). The $Sum(\tilde{\mathcal{W}}_{d(3 \times 3)})$ is given as:

$$Sum(\tilde{\mathcal{W}}_{d(3 \times 3)}) = \sum_{i=g}^{g+2} \sum_{j=d}^{d+2} \check{X}_{\tilde{\alpha}+\tilde{i},\tilde{\alpha}+\tilde{j}} \quad (9)$$

$$\text{for } g = 0, 1, 2, 3, \dots, l-2 \text{ \& } d = 0, 1, 2, 3, \dots, t-2$$

Furthermore, the $\vartheta_{\tilde{\mathcal{W}}_{d(3 \times 3)}}$ is the sum of F_{rv} and $\check{I}_{min,max}$. Whereas the F_{rv} is the addition of total ratio value of $\check{R}_{\tilde{\mathcal{W}}_{d(3 \times 3)}}$ in $\tilde{\mathcal{W}}_{d(3 \times 3)}$ and $\check{I}_{min,max}$ is the ratio of minimum to maximum intensity with in $\tilde{\mathcal{W}}_{d(3 \times 3)}$. When \mathcal{X}_s are obtained, then the use $\vartheta_{\tilde{\mathcal{W}}_{d(3 \times 3)}}$ enhances their visibility, also helping them to stand out more from background or noise. Without applying $\vartheta_{\tilde{\mathcal{W}}_{d(3 \times 3)}}$, the pixel values may reduce significantly or may tiny or almost zero. Therefore, algorithm 1 illustrates the process of pixel augmentation of an image using a 3×3 window.

Algorithm 1: Pixel augmentation using 3×3 window

1. Input: Image of size $l \times t$
2. Output: Augmented pixels \mathcal{X}_s using $\tilde{\mathcal{W}}_{d(3 \times 3)}$
3. Initialization Parameters:
 - a. Size of window is 3, row and column are represented with \tilde{i} & \tilde{j} respectively
4. Procedure:
 - Start iteration:
 - a. Outer Loop: Iterate over row (\tilde{i}):
 $\tilde{i} = g$ to $g + 2$ %% $g = 0, 1, 2, \dots, l - 2$
 - b. Inner Loop: Iterate over columns (\tilde{j}):
 $\tilde{j} = d$ to $d + 2$ %% $d = 0, 1, 2, \dots, t - 2$
 - c. Extract the current 3×3 window:
 $\tilde{\mathcal{W}}_{d(3 \times 3)} = [\check{X}_{\tilde{\alpha}+\tilde{i},\tilde{\alpha}+\tilde{j}}]$ %% Using eqn. (6)
 - d. Compute: $\check{R}_{\tilde{\mathcal{W}}_{d(3 \times 3)}}$, $Sum(\tilde{\mathcal{W}}_{d(3 \times 3)})$ and $\vartheta_{\tilde{\mathcal{W}}_{d(3 \times 3)}}$
 - e. Compute the augmented scaling factor:
 $\tilde{A}\hat{S}_{fa} = \check{X}_{\tilde{\alpha}+\tilde{i},\tilde{\alpha}+\tilde{j}} = [\vartheta_{\tilde{\mathcal{W}}_{d(3 \times 3)}} + \check{R}_{\tilde{\mathcal{W}}_{d(3 \times 3)}}]$
 - f. Compute the final augmented pixel's values:
 $\mathcal{X}_s = [\tilde{A}\hat{S}_{fa}] \times [\check{X}_{\tilde{\alpha}+\tilde{i},\tilde{\alpha}+\tilde{j}}]$ %% Using eqn. (7)
 - Complete iteration:
 - a. The window automatically shifts by incrementing \tilde{j} within the inner loop
 - b. After completing a row, increment \tilde{i} to move to next row
 - c. The algorithm terminates when last column ($\tilde{j} = d$ to $d + 2$) and last row ($\tilde{i} = g$ to $g + 2$) are reached or processed
5. The result represents the augmented pixels (\mathcal{X}_s) for complete image $l \times t$. Further these pixels applied in segmentation process.

The Pixel augmentation enhances the visual quality of road images, improving their clarity and detail. By boosting contrast, emphasizing edges, and preserving essential features, it makes road cracks more distinguishable. This pre-processed image is subsequently input into PIEFCMC, facilitating a more precise distinction between crack and non-crack regions. This process reduces false positives and ensures consistent segmentation accuracy, even in the presence of noise, uneven lighting, and surface irregularities.

3.3 Exhaustive description of the PIEFCMC

The objective function (η) of the reliable & effective PIEFCMC approach for the successful identification of road fractures can be articulated as follows:

$$\eta(\psi, \mathcal{Y}) = \sum_{e=1}^{\mathfrak{v}} \sum_{s=1}^m \psi_{es}^c \times \|\mathcal{X}_s - \mathcal{Y}_e\|^2 \times \mathring{A}_{d(max.,s)}(s) \quad (10)$$

where \mathfrak{v} & m stand for the number of clusters for partitioning the data and pixels in a picture, \mathcal{X}_s represent the augmented image pixels, \mathcal{Y}_e is cluster center, c is fuzzification parameter ($(c > 1)$ and controls the degree of cluster overlap), ψ_{es} is the fuzzy membership matrix quantify the degree to which each data point belongs to each cluster. The $\mathring{A}_{d(max.,s)}(s) (= |\mathcal{X}_{max.} - \mathcal{X}_s|)$ stands for absolute intensity difference between maximum pixel intensity and all the other pixels.

The utilization of the $\mathring{A}_{d(max.,s)}(s)$ function enables the proposed algorithm possible to observe the intrinsic connection between the pixels in $l \times t$ picture. It measures how each pixel deviates from the most prominent intensity, establishing a relative scale of connection. This process help in grouping similar pixels, while isolating dissimilar ones, thereby reducing noise, enhances clarity, ultimately improving segmentation accuracy.

After that employing *Lagrange multiplier method* to reducing the objective function $\eta(\psi, \mathcal{Y})$, that may ascertain the revised membership degrees and cluster centers in PIEFCMC, as follows:

$$\zeta_{multiplier} = \sum_{e=1}^{\mathfrak{v}} \sum_{s=1}^m \psi_{es}^c \times \|\mathcal{X}_s - \mathcal{Y}_e\|^2 \times \mathring{A}_{d(max.,s)}(s) + \sum_{s=1}^m \nabla \left(1 - \sum_{e=1}^{\mathfrak{v}} \psi_{es} \right) \quad (11)$$

Utilizing partial derivative on $\zeta_{multiplier}$ with regards to ψ_{se}^c & subsequently setting it to zero, we arrive:

$$\psi_{es} = \left(\frac{\nabla}{c(\|\mathcal{X}_s - \mathcal{Y}_e\|^2 \times \mathring{A}_{d(max.,s)}(s))} \right)^{\frac{1}{c-1}} \quad (12)$$

Utilizing the $\zeta_{multiplier}$ derivative in relation to the ∇ (Lagrange multipliers), the following results are obtained:

$$\frac{\partial \zeta_{multiplier}}{\partial \nabla} = \sum_{e=1}^{\mathfrak{v}} \psi_{es} - 1 = 0 \quad (13)$$

To ascertain the membership function, solve the eqn. no. 12-13 and yield the following result:

$$\psi_{es} = \frac{\left[\frac{1}{\partial_{es}} \right]^{\frac{1}{c-1}}}{\sum_{\#s=1}^{\mathfrak{v}} \left[\frac{1}{\partial_{\#s}} \right]^{\frac{1}{c-1}}} \quad (14)$$

Likewise, obtaining the cluster centroid's the partial derivative of $\zeta_{multiplier}$ with regard to \mathcal{Y}_e is provides as:

$$\frac{\partial \zeta_{multiplier}}{\partial \mathcal{Y}_e} = 0 \quad (15)$$

After the aforementioned equation is extricate, the centroid is eventually obtained as follows:

$$\mathcal{Y}_e = \frac{\sum_{s=1}^m \psi_{es}^c \times \mathcal{X}_s \times \mathring{A}_{d(max.,s)}(s)}{\sum_{s=1}^m \psi_{es}^c} \quad (16)$$

The algorithm 2 is on PIEFCM clustering are given below:

Algorithm 2: PIEFCM clustering algorithm

1. Input: Size of image $l \times t$
2. Output: %% Identification of the cracks on road
3. Initialization Parameters:
 - a. \mathfrak{v} is number of clusters, \mathcal{X}_s represent the augmented image pixels, m is the total number of pixels in picture, \mathcal{Y}_e is cluster center, c is fuzzification parameter, ψ_{es} the fuzzy membership matrix
4. Procedure:
 - 4.1. Outer Loop (e): Iterate for \mathfrak{v} %% Start iteration over cluster
 - 4.2. Inner Loop (s): Iterate for m %% Start iteration over pixels
 - 4.3. Membership matrix is randomly initialization in the beginning: $\psi_{es} = 1$
%% $\psi = [\psi_{es}]_{\mathfrak{v} \times m}$ with $0 \leq \psi_{es} \leq 1$
 - 4.4. Exit inner loop: When $s=m$; %% Stop iterating over pixels
 - 4.5. Exit outer loop: When $e=\mathfrak{v}$; %% Stop iterating over clusters
 - 4.6. Initialize: $\mathring{y}=0$ %% \mathring{y} =iteration index
 - 4.7. Outer Loop (e): Iterate for \mathfrak{v} %% Start iteration over clusters
 - 4.8. Inner Loop (s): Iterate for m %% Start iteration over pixels

4.9. Compute \mathbb{Y}_e : $\mathbb{Y}_e =$

$$\frac{\sum_{s=1}^m \psi_{es}^c \times \mathcal{X}_s \times \mathring{A}_{d(max.,s)}(s)}{\sum_{s=1}^m \psi_{es}^c} \quad \mathring{A}_{d(max.,s)}(s) (=$$

$$|\mathcal{X}_{max.} - \mathcal{X}_s|)$$

4.9.1. Condition: For $\mathring{A}_{d(max.,s)}(s) \quad \mathring{A}_{d(max.,s)}(s)$ *Absolute intensity difference*

4.9.1.1. If $\mathring{A}_{d(max.,s)}(s) \neq 0$; then

$$\mathring{A}_{d(max.,s)}(s) = |\mathcal{X}_{max.} - \mathcal{X}_s|$$

else ($\mathring{A}_{d(max.,s)}(s) = 0$)

$\mathring{A}_{d(max.,s)}(s) = A_v(\mathcal{X}_{max.}, \mathcal{X}_s)$ *Average (A_v) between $\mathcal{X}_{max.}$ and \mathcal{X}_s*

4.10. Calculate and update ψ_{es} :

$$\psi_{es} = \frac{\left[\frac{1}{\partial_{es}}\right]^{c-1}}{\sum_{\neq=1}^{\mathring{v}} \left[\frac{1}{\partial_{\neq e}}\right]^{c-1}}$$

$$\mathring{v} \quad \partial_{es} = \|\mathcal{X}_s - \mathbb{Y}_e\|$$

4.11. Exit inner loop: When $s=m$; *stop iterating over pixels*

4.12. Exit outer loop: When $e=\mathring{v}$; *stop iterating over clusters*

4.13. Repetation or convergence criteria: Increment $\mathring{y} = \mathring{y} + 1$ or revisit steps 4.7 until an identical \mathbb{Y}_e emerges, or Max. $\|\boldsymbol{\psi}^{(\mathring{y}+1)} - \boldsymbol{\psi}^{(\mathring{y})}\| < \alpha$, where α is positive threshold termination criteria.

5. Output: Cracks identification from complete $l \times t$ image

wherein the road endures to intense stress, a \mathring{T}_{crk} may emerge. \mathring{A}_{crk} may appear mainly due to inadequate strength in the asphalt substrate. When precipitation penetrates the earth underlying the roadway's exterior and expands and contracts, it impacts substantial structural degradation in the form of \mathring{P}_{ot} [13]. Hence for crack types, we personally gathered the dataset from National Highway (NH)-154 in Himachal Pradesh, India, from whence these pictures are taken. Samsung's 64-megapixel camera was used to take these photos.

The suggested procedure has been contrasted to anterior methods, specifically KMC [7][8], FCMC [9][4], and MHFCMC [10]. Utilising self-gathered datasets consists of non-tainted and tainted road photos, PIEFCMC performs more effectively in terms of number of iterations, precision, recall, and F1 Score. The superior performance of this can be attributed to its innovative use of pixel enhancement and absolute intensity difference in segmentation process, as discussed in Section 3. This unique approach effectively reduces noise and improves the clarity and visibility of detected road cracks, offering a significant advantage over K-Means, FCMC, and MHFCMC, whose limitations are outlined in Section 2.

Additionally, we recognize that no method is flawless. Hence, PIEFCMC may also faces performance limitations in the situations where road cracks are extremely faint or image quality is highly compromised or instances of severe occlusion. Therefore, the experimental analysis is explained in detail in subsections 4.1 and 4.2, respectively, offering a description of the empirical outcomes for the two aforementioned photo genres.

4 Experimental result and analysis

This section analyses and juxtaposes /compares the outcomes of the PIEFCMC method with a number of other methods that are implemented in Matlab, such as KMC, FCMC, MHFCMC. A central processing unit (CPU) of Intel Core i7, 1.80 GHz of clock speed, Random-access memory (RAM) of 8.00 GB, and Microsoft Windows 11 Pro are the specifications of the personal computer (PC) used for this assessment. The performance of the suggested approach is primarily influenced by the parameters c and \mathring{v} , which have been assigned values of 2 each. Therefore, by using these parameters, fractures may be clearly distinguished among their adjacent regions during the detecting procedure. This facilitates a clear division into two clusters: one for crack areas and the other for non-crack regions. Consequently, all variations of the fuzzy algorithms in our simulation operate under these similar conditions.

In this simulation a numerous number of road photos exhibiting numerous varieties of flaws and fractures, including transverse crack (\mathring{T}_{crk}), longitudinal crack (\mathring{L}_{crk}), alligator fractures (\mathring{A}_{crk}) and pathole (\mathring{P}_{ot}). Excessive exhaustion and insufficient articulation cause the \mathring{L}_{crk} to emerge longitudinally along the road [16]. When an articulation is positioned within a vicinity

4.1 Non-Tainted images of road

A non-contaminated road crack image is free from oil stains, paint, mud, and other obstructions for analysis. The analysis contrasts the KMC, FCMC, MHFCMC, and PIEFCMC for the various visual formats shown in Figures 3(a), 4(a), 5(a), and 6(a). In juxtaposition with MHFCMC, KMC and FCMC yield inferior results for road fracture identification as shown in Fig. 3-6: (b-d). However, the MHFCMC displays relatively little disturbance and has trouble diagnosing fractures, shown in Fig. 3-6: (d)). Regarding noise, reliability, and iterations, the PIEFCMC approach's output (Fig. 3(e)–6(e)) offers superior and valuable results in lieu of the other methods. In addition, the PIEFCMC can distinguish between cracked and non-crack pixels with ease.

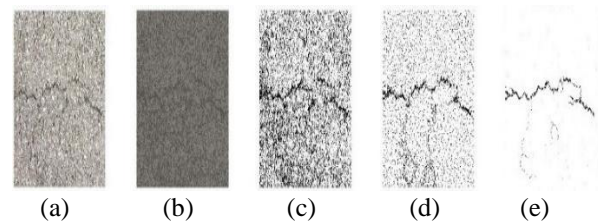


Figure 3. Detection results of \check{T}_{crk} : (a) Original image, (b) KMC, (c) FCMC, (d) MHFCMC, (e) PIEFCMC

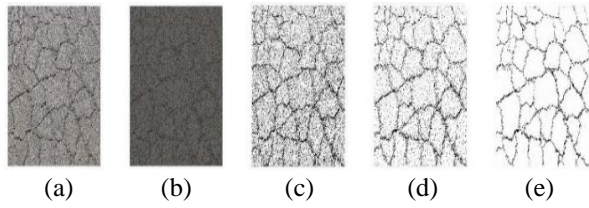


Figure 4. Detection results of \check{A}_{crk} : (a) Original image, (b) KMC, (c) FCMC, (d) MHFCMC, (e) PIEFCMC

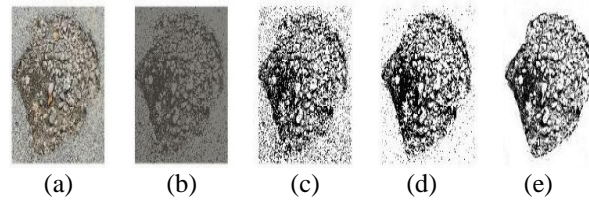


Figure 5. Detection results of \check{P}_{oi} : (a) Original image, (b) KMC, (c) FCMC, (d) MHFCMC, (e) PIEFCMC

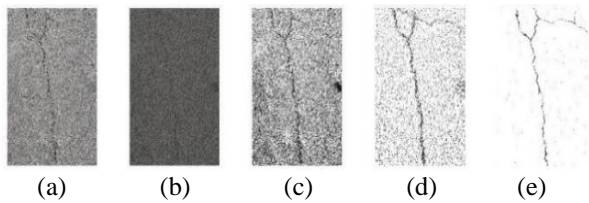
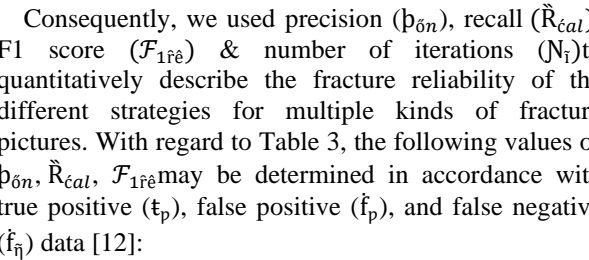


Figure 6. Detection results of \check{L}_{crk} : (a) Original image, (b) KMC, (c) FCMC, (d) MHFCMC, (e) PIEFCMC



Consequently, we used precision ($p_{\delta n}$), recall (\check{R}_{cal}), F1 score ($\mathcal{F}_{1\hat{r}\hat{e}}$) & number of iterations (N_i) to quantitatively describe the fracture reliability of the different strategies for multiple kinds of fracture pictures. With regard to Table 3, the following values of $p_{\delta n}$, \check{R}_{cal} , $\mathcal{F}_{1\hat{r}\hat{e}}$ may be determined in accordance with true positive (t_p), false positive (f_p), and false negative ($f_{\bar{n}}$) data [12]:

$$p_{\delta n} = \frac{t_p}{t_p + f_p} \tag{17}$$

$$\check{R}_{cal} = \frac{t_p}{t_p + f_{\bar{n}}} \tag{18}$$

$$\mathcal{F}_{1\hat{r}\hat{e}} = \frac{2 \times p_{\delta n} \times \check{R}_{cal}}{p_{\delta n} + \check{R}_{cal}} \tag{19}$$

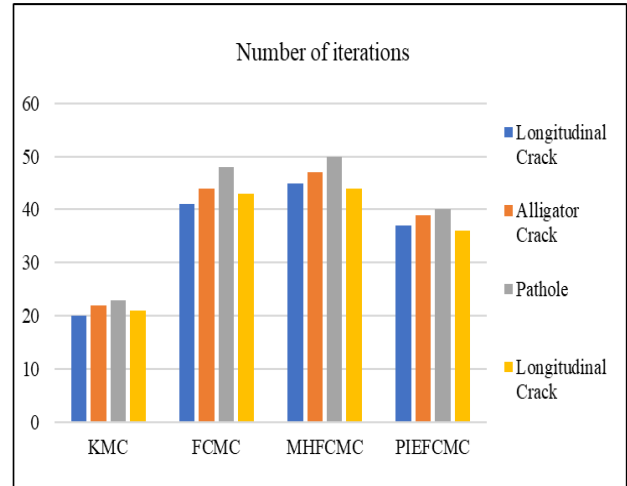


Figure 7: Number of iterations across multiple algorithms for detecting various kind of cracks in non-tainted images

The PIEFCMC contain an efficient pixel augmentation with neighborhood relationshipoutperforms various other algorithm in terms of $p_{\delta n}$, \check{R}_{cal} , & $\mathcal{F}_{1\hat{r}\hat{e}}$ for all sorts of fractures, hence offering effective information on fracture recognition. The KMC method boasts a shorter N_i in comparison to its counterparts. However, the simulation results reveal its underperformance in terms of $p_{\delta n}$, \check{R}_{cal} , $\mathcal{F}_{1\hat{r}\hat{e}}$. Hence, based on the comprehensive findings presented in Table 3 and Figure 7, it is apparent that PIEFCMC demonstrates superior efficiency for N_i when compared with other's.

4.2 Tainted images of road

This section delves into the discussion of various categories of imperfections and fissures observed in photos of tainted roadways, including paint marks, mud and shadows, etc. The findings entail a comparison of several algorithms across varied visuals, as depicted in Figures 8(a), 9(a), 10(a), and 11(a). The findings indicate that MHFCMC outperforms the KMC and FCMC algorithms in terms of efficacy, as is evident in Figures 8–11 (b–d). As seen in Figures 8(d)–11(d), MHFCMC, however, exhibits significant shortcomings, including poor responsiveness, noise, shadow traces, and blurring, especially in comparison to PIEFCMC. The PIEFCMC approach surpasses comparable algorithms in regard of noise reduction, precision and execution time and identifies boundaries from the vicinity with efficacy.

Table 3: Comparative analysis of crack identification performance between KMC, FCMC, MHFCMC and PIEFCMC for non-tainted images

Crack Types	Parameters	KMC	FCMC	MHFCMC	PIEFCMC
\check{T}_{crk}	$\check{p}_{\check{o}n}$	74.07	78.57	83.90	85.95
	$\check{R}_{\check{c}al}$	75.94	80.48	84.88	88.43
	$\mathcal{F}_{1\check{r}\check{e}}$	74.99	79.51	84.38	87.17
	$N_{\check{I}}$	20	41	45	37
\check{A}_{crk}	$\check{p}_{\check{o}n}$	76.82	79.76	84.09	86.68
	$\check{R}_{\check{c}al}$	78.05	80.72	86.14	88.53
	$\mathcal{F}_{1\check{r}\check{e}}$	77.43	80.23	85.10	87.59
	$N_{\check{I}}$	22	44	47	39
$\check{P}_{\check{o}t}$	$\check{p}_{\check{o}n}$	76.96	77.64	83.33	82.95
	$\check{R}_{\check{c}al}$	78.39	75.86	81.39	85.88
	$\mathcal{F}_{1\check{r}\check{e}}$	77.66	76.73	82.34	84.38
	$N_{\check{I}}$	23	48	50	40
\check{L}_{crk}	$\check{p}_{\check{o}n}$	72.83	78.57	83.48	84.44
	$\check{R}_{\check{c}al}$	75.64	80.48	85.97	86.36
	$\mathcal{F}_{1\check{r}\check{e}}$	74.20	79.51	84.70	85.38
	$N_{\check{I}}$	21	43	44	36

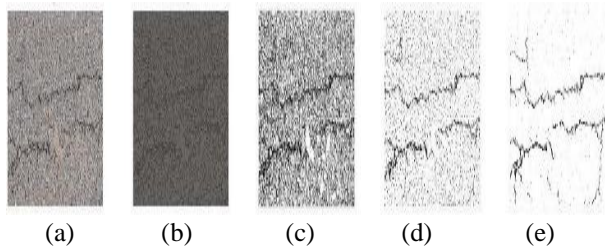


Figure 8: Detection results of \check{T}_{crk} : (a) Original image, (b) KMC, (c) FCMC, (d) MHFCMC, (e) PIEFCMC

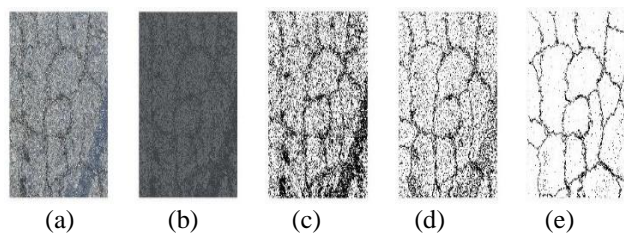


Figure 9: Detection results of \check{A}_{crk} : (a) Original image, (b) KMC, (c) FCMC, (d) MHFCMC, (e) PIEFCMC

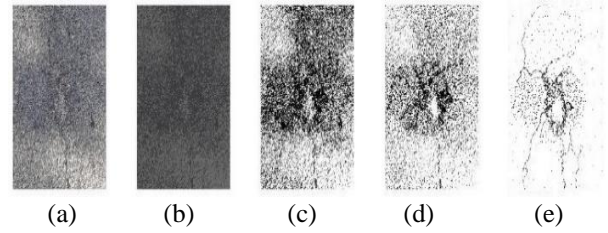


Figure 10: Detection results of $\check{P}_{\check{o}t}$: (a) Original image, (b) KMC, (c) FCMC, (d) MHFCMC, (e) PIEFCMC

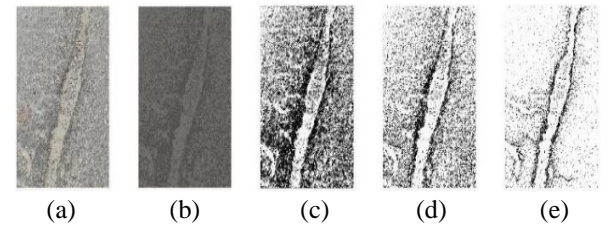


Figure 11: Detection results of \check{L}_{crk} : (a) Original image, (b) KMC, (c) FCMC, (d) MHFCMC, (e) PIEFCMC

Table 4: Comparative analysis of crack identification performance between KMC, FCMC, MHFCMC and PIEFCMC for tainted images

Crack Types	Parameters	KMC	FCMC	MHFCMC	PIEFCMC
\check{T}_{crk}	$\check{p}_{\check{o}n}$	71.12	76.84	80.40	82.51
	$\check{R}_{\check{c}al}$	72.98	77.37	83.02	84.95
	$\mathcal{F}_{1\check{r}\check{e}}$	72.03	77.10	81.68	83.71
	$N_{\check{I}}$	22	42	46	38
\check{A}_{crk}	$\check{p}_{\check{o}n}$	72.67	76.05	81.76	83.32
	$\check{R}_{\check{c}al}$	74.98	78.67	83.24	85.35
	$\mathcal{F}_{1\check{r}\check{e}}$	73.80	77.33	82.49	84.32
	$N_{\check{I}}$	24	46	49	40
$\check{P}_{\check{o}t}$	$\check{p}_{\check{o}n}$	70.06	74.93	77.83	80.47
	$\check{R}_{\check{c}al}$	68.35	72.49	79.18	82.93
	$\mathcal{F}_{1\check{r}\check{e}}$	69.19	73.68	78.49	81.68
	$N_{\check{I}}$	23	44	47	37
\check{L}_{crk}	$\check{p}_{\check{o}n}$	72.98	75.64	79.98	81.83
	$\check{R}_{\check{c}al}$	73.57	77.59	81.48	83.47
	$\mathcal{F}_{1\check{r}\check{e}}$	73.27	76.60	80.72	82.64
	$N_{\check{I}}$	21	45	48	39

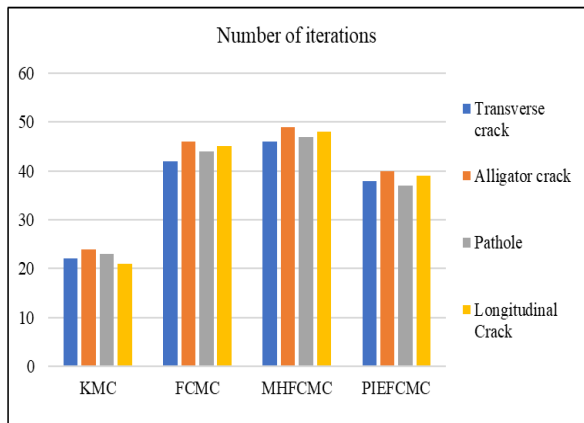


Figure 12: Number of iterations across multiple algorithms for detecting various kind of cracks in tainted images

The Equations 17-19 have been utilised in the current model for determining the $\beta_{\delta n}$, \tilde{R}_{cal} and \mathcal{F}_{1re} for crack accuracy; the outcomes are depicted in Table 4. The Table 4 indicates that PIEFMC trumps all variants, allowing effective recognition of fractures in spite of tainted photos.

Additionally, the KMC approach executes more quickly than the others—including PIEFMC—it performs noticeably worse overall. On the other hand, as Figure 12 illustrates, PIEFMC provides an accurate, efficient and effective N_T for the entire operation then other.

4.3 Comparison between proposed PIEFMC and Deep Learning based approaches

The proposed PIEFMC algorithm offers several benefits over deep learning-based approaches such as Convolutional Neural Networks (CNNs). Unlike CNNs, which require large labeled datasets and high-performance hardware, PIEFMC operates efficiently with smaller datasets [25] and standard hardware, such as a CPU. It has a substantially lower computational cost than CNNs. Additionally, CNNs require intensive and time-consuming training process, but PIEFMC does not require a training phase. Additionally, CNNs are frequently limited in their interpretability [25], whereas PIEFMC is extremely interpretable. However, CNNs can achieve higher accuracy and adaptability for complex patterns, especially when trained on diverse datasets, making them suitable for highly precise tasks [25][26]. Thus, PIEFMC serves as a cost-effective and efficient alternative, especially in scenarios with limited resources or data.

4.4 Discussions

The experimental findings unequivocally demonstrate the efficacy of the proposed PIEFMC algorithm in accurately detecting road cracks from both tainted and non-tainted images. This innovative approach employs a 3×3 window with a scaling factor

for pixel enhancement, effectively utilizing absolute intensity differences to emphasize finer details while significantly mitigating noise. These features address critical limitations evident in previously reviewed methods, establishing PIEFMC as a robust and effective solution.

In comparison, existing methods such as KMC, FCMC, and MHFCMC exhibit notable shortcomings that limit their effectiveness. KMC's reliance on pre-defined clusters hinders its adaptability to intricate data, compromising precision. FCMC, is highly susceptible to noise due to its disregard for spatial pixel connectivity, resulting in reduced reliability. MHFCM faces processing challenges, due to complexities associated with FCM and histogram equalization.

The superiority of PIEFMC is particularly evident in its performance metrics. For tainted images, PIEFMC achieves precision, recall, and F1 scores of 86.68, 88.53, and 87.59, respectively, outperforming KMC (76.82, 78.05, 77.43), FCMC (79.76, 80.72, 80.23), and MHFCMC (84.09, 86.14, 85.10). Similarly, for non-tainted images, PIEFMC achieves precision, recall, and F1 scores of 83.32, 85.35, and 84.32, surpassing KMC (72.67, 74.98, 73.80), FCMC (76.05, 78.67, 77.33), and MHFCMC (81.76, 83.24, 82.49). These results highlight PIEFMC's consistent accuracy and reliability across diverse image conditions.

Another significant advantage of PIEFMC lies in its optimized iteration count. While KMC demonstrates the fewest iterations for tainted (21) and non-tainted (20) images, this efficiency comes at the cost of reduced segmentation accuracy. In contrast, PIEFMC achieves a balance between iteration count and performance, requiring 37 iterations for tainted images and 36 for non-tainted images while delivering superior precision and reliability. FCMC and MHFCMC, on the other hand, require 41–46 iterations, further underscoring the computational efficiency of PIEFMC.

In conclusion, PIEFMC significantly advances the field of road crack detection by delivering higher precision, recall, and F1 scores while effectively addressing noise and computational challenges. Although it slightly lags behind KMC in iteration count, its superior segmentation accuracy, robustness, and consistency across varying image types validate its potential as a transformative approach in this domain.

5 Conclusion and future research directions

This study presents a novel and innovative method for road fracture identification based on FCM clustering. Despite the dearth of research on the application of the FCM algorithm to road crack identification. Still, this approach reduces the effect of noise and finds road fractures in images better than FCM and its variants. To achieve this, a 3×3 window is spans across the entire image. This approach enables the enhancement of pixel technique within each window, effectively emphasizing the finer details of cracks. By this method, each pixel in the 3×3 window is considered based on the sum of the

values of its neighboring pixels prior to segmentation. In situation, when initial pixel values are little or almost zero, $\vartheta_{\mathcal{W}_{d(3 \times 3)}}$ helps draw attention to them by making them stand out contrary to noise or the backdrop, which improves contrast among various areas or entities in the picture. Furthermore, this strategy allows the observation of the intrinsic connection among the photograph's pixels because of the absolute difference. Consequently, the innovative methodology markedly enhances clustering, precision meticulously delineates boundaries, and effectively eradicates blurring, culminating in substantially superior outcomes. Even in images characterized by low contrast, it adeptly identifies cracks and edges. Unlike many FCM variations, the novel strategy eradicates the need for determining the crucial tuning parameters, and experimental results confirm that it consistently produces better results. Moreover, without the exigency to training dataset, the novel algorithm can accurately recognize fractures in novel, unseen images of diverse types. The comprehensive test findings demonstrate the effectiveness of the novel algorithm in terms of $\mathfrak{p}_{\delta n}$, $\mathfrak{R}_{\text{cal}}$, $\mathcal{F}_{1\text{re}}$ and iteration count. As a result, PIEFCMC exhibits exceptional effectiveness in identifying different types of road cracks, saving a substantial sum of money and effort.

The upcoming task entails installing a state-of-the-art online embedded device with premium webcams in cars. The gathering and accumulation of immediate video streams will be made possible by this upgrade. Furthermore, utilising real-time data streams, a customised methodology will be developed to determine the width and depth of road fractures. Also, the proposed method's performance under rainy conditions has not been considered in the current work due to the unavailability of datasets. Consequently, we have not utilized such images in any experiments. However, we intend to thoroughly explore this aspect in our future research. Moving forward, integrating PIEFCMC (an unsupervised machine learning approach) with other machine learning techniques could further improve the accuracy and robustness of road crack detection.

References

- [1] Diahao Ai, Guiyuan Jiang, Lam Siew Kei and Chengwu Li. Automatic pixel-level pavement crack detection using information of multi-Scaleneighborhoods. *IEEE access*, 6: 24452-24463, 2018. <https://doi.org/10.1109/ACCESS.2018.2829347>
- [2] Arun Mohan, Sumathi Poobal. Crack Detection using image processing: A critical review and analysis. *Alexandria engineering journal*, 57(2): 787-798, 2018. <https://doi.org/10.1016/j.aej.2017.01.020>
- [3] Yuming Zhang, Cong Chen, Qiong Wu, Qi Lu, Su Zhang, Guohui Zhang. A Kinect-Based approach for 3D pavement surface reconstruction and cracking recognition. *IEEE transactionson intelligent transportation systems*, 19(12):3935-3946, 2018. <https://doi.org/10.1109/TITS.2018.2791476>
- [4] Dan Wang, Zaijun Zhang, Jincheng Zhou, Benfei Zhang, and Mingjiang Li. Comparison and analysis of several clustering algorithms for pavement crack segmentation guided by computational intelligence. *Hindawicomputational intelligence and neuroscience*, 2022(12):1-13, 2022. <https://doi.org/10.1155/2022/8965842>
- [5] Munish Bhardwaj, Nafis Uddin Khan, Vikas Baghel. Fuzzy C-Means clustering based selective edge enhancement scheme for improved road crack detection. *Engineering applications of artificial intelligence*, 136 (A): 1-14, 2024. <https://doi.org/10.1016/j.engappai.2024.108955>
- [6] Vidya Dhanve, Meeta Kumar. Detection of brain tumor using k-means segmentation based on object labeling algorithm. *IEEE international conference on Power, Control, Signals and Instrumentation engineering*, 944–951, 2017. <https://doi.org/10.1109/ICPCSI.2017.8391851>
- [7] Abdul Rahim Ahmad, MuhammandKhusairi Osman, K. A. Ahmad, M. A. Anuar, Nor Aizam Muhamed Yusof. Image segmentation for pavement crack detection system. *IEEE international conference on control system, computing and engineering*, 153-157, 2020. <https://doi.org/10.1109/ICCSCCE50387.2020.9204935>
- [8] Munish Bhardwaj, Nafis Uddin Khan, Vikas Baghel, Santosh Kumar Vishwakarma, and Abul Bashar. Brain tumor image segmentation using K-means and FuzzyC-Means clustering. *Digital image enhancement and reconstruction elsevierinc.*, 293-316, 2023. <https://doi.org/10.1016/B978-0-32-398370-9.00020-2>
- [9] James C. Bezdek, Robert Ehrlich, Willam Full. FCM: The Fuzzy C-Means clustering algorithm. *Computers & geosciences*, 10 (2-3): 191-203, 1984. [https://doi.org/10.1016/0098-3004\(84\)90020-7](https://doi.org/10.1016/0098-3004(84)90020-7)
- [10] Munish Bhardwaj, Nafis Uddin Khan, Vikas Baghel. Improved road crack detection using Histogram Equalization based Fuzzy-C Means technique. *IEEE conference on PDGC*, 547-551, 2023. <https://doi.org/10.1109/PDGC56933.2022.10053319>
- [11] Yohwan Noh, Donghyun Koo, Yong-Min Kang, Dong Gyu Park, DoHoon Lee, Panop Khumsap. Automatic crack detection on concrete images using segmentation via Fuzzy C-means clustering. *IEEEinternational conference on applied system innovation*, 877-880, 2017. <https://doi.org/10.1109/ICASI.2017.7988574>
- [12] Munish Bhardwaj, Nafis Uddin Khan, Vikas Baghel. Road crack detection using pixel

- classification and intensity-based distinctive Fuzzy C-means clustering. *The visual computer*,41:1689–1704,2024.
<https://doi.org/10.1007/s00371-024-03470-8>
- [13] Yashon O. Oumaa, M. Hahn. Pothole detection on asphalt pavements from 2D-colour pothole images using Fuzzy c-means clustering and morphological reconstruction. *Automation and construction*, 83: 196-211,2017.
<https://doi.org/10.1016/j.autcon.2017.08.017>
- [14] S. Mubashshira, M. M. Azam and S. M. Masudul Ahsan. An unsupervised approach for road surface crack detection. *IEEE region 10 symposium (TENSYP)*,1596-1599, 2020.
<https://doi.org/10.1109/TENSYP50017.2020.9231023>
- [15] Amita Nandal, Vidhyacharan Bhaskar. Fuzzy enhanced image fusion using pixel intensity control. *IET image processing*, 12(3):453-464, 2018.
<https://doi.org/10.1049/iet-ipr.2017.0405>
- [16] A. Cubero Fernandez, Fco. J. Rodriguez Lozano, Rafael Villatoro, Joaquin Olivares and Jose M. Palomares. Efficient pavement crack detection and classification. *EURASIP journal on image and video processing*, 39:1-11, 2017.
<https://doi.org/10.1186/s13640-017-0187-0>
- [17] Yong Shi, Limeng Cui, Zhiquan Qi, Fan Meng, and Zhensong Chen. Automatic road crack detection using Random Structured Forests. *IEEE transactions on intelligent transportations systems*, 17(12):3434-3445, 2016.
<https://doi.org/10.1109/TITS.2016.2552248>
- [18] Abdulrahman Tawfeeq Azeez, N. Anupama. Crack pavement detection utilizing Fuzzy Inference System. *IJSETR*, 5(7):1400-1404, 2016.
<https://doi.org/10.13140/RG.2.2.31345.60004>
- [19] Weixing Wang, Lei Li, Ya Han. Crack detection in shadowed images on gray level deviations in a moving window and distance deviations between connected components. *Construction and building material elsevier*, 271: 1-12, 2021.
<https://doi.org/10.1016/j.conbuildmat.2020.121885>
- [20] Jie Luo, Huazhi Lin, Xiaoxu Wei and Yongsheng Wang. Adaptive Canny and Semantic segmentation Networks based on Feature Fusion for road crack detection. *IEEE access*,11:51740-51753, 2023.
<https://doi.org/10.1109/ACCESS.2023.3279888>
- [21] Junde Chen, Yuxin Wen, Yaser Ahangari Nanekaran, Defu Zhang, and Adan Zeb. Multi-scale attention networks for pavement defect detection. *IEEE transactions on instrumentation and measurement*, 72:1-12, 2023.
<https://doi.org/10.1109/TIM.2023.3298391>
- [22] Rafael C. Gonzalez, Richrad E Woods. *Digital image processing*. Pearson Hall, 2002.
- [23] Džulijana Popović, Bojana Dalbelo Bašić. Churn prediction model in retail banking using Fuzzy C-Means Algorithm. *Informatica*, 243-247, 2009.
- [24] Youmeng Guan. An algorithm for data management of higher education based on Fuzzy Set Theory - association rule mining algorithm. *Informatica*, 45 (2021):157–164, 2023.
<https://doi.org/10.31449/inf.v47i9.5222>
- [25] Yujun Wang. Deep Learning models in computer data mining for intrusion detection. *Informatica*, 47:555–568, 2023.
<https://doi.org/10.31449/inf.v47i4.4942>
- [26] Ming Zhu, Yongning He, Qingyu He. A review of researches on Deep Learning in Remote Sensing application. *International journal of geosciences*, 10(1) :1-11, 2019.
<https://doi.org/10.4236/ijg.2019.101001>

